Research Article | DOI:10.5281/zenodo.10372139
www.jnanosam.com

NANOSAM
Journal of NanoScience in Advanced Materials

In situ Synthesis of 2D Bismuth/Graphitic Carbon Nitride Heterojunctions for the Visible Light-Driven Organic Dye Degradation

Buse Sündü[1], Ayben Türkkan[1], Zafer Eroglu[1#], Onder Metin[1,2#]

In this study, highly efficient photocatalysts were developed by synthesizing binary heterojunctions of 2D Bismuth/Graphitic Carbon Nitride (2D Bi/gCN) in various ratios through a facile *in situ* synthesis method. Advanced analytical techniques were used to characterize the yielded heterojunctions, and their photocatalytic performance was evaluated in the Methyl Orange (MO) degradation under visible light irradiation. The 2D Bi/gCN heterojunctions provided exceptional photoactivity under visible light illumination, leading to the significantly higher degradation efficiency compared to pristine gCN. To clarify the high photocatalytic dye degradation activity of 2D Bi/gCN heterojunctions, a band diagram that depicts the dynamics of electron-hole migration between the gCN and 2D Bi in the heterojunction structure revealed the formation of a type-I heterojunction. The photophysical and structural characteristics of the 2D Bi/gCN heterojunctions were assessed by utilizing different approaches to authenticate the effective integration of 2D Bi into gCN layers. The 2D Bi/gCN heterojunctions exhibit enhanced light absorption and improved charge separation, with the 2D $Bi_{0.06}$/gCN composition exhibiting the highest photocatalytic performance, achieving 61% MO photodegradation efficiency in 30 min. Kinetic analysis demonstrated that the 2D $Bi_{0.06}$/gCN composition degraded MO at a rate 2.04 times higher than pristine gCN. Overall, the 2D Bi/gCN heterojunctions showed promising photocatalytic properties with the 2D $Bi_{0.06}$/gCN heterojunctions emerging as an exceptionally efficient photocatalyst for MO degradation under visible light illumination. This research contributes to the understanding and application of 2D Bi/gCN heterojunctions as photocatalysts in the development of other sustainable chemical processes.

1. Introduction

With the development of technology, the pervasive issue of environmental pollution has come to the forefront [1]. Rapidly growing industry and the increasing population are among the major factors causing environmental pollution [2]. Water pollution, in particular, poses a significant threat to human health and conventional water treatment methods often fall short of completely removing contaminants, leading to the persistent presence of pollutants in various water bodies [3]. The majority of water pollution is caused by dyes due to their widespread use in various sectors. Among these dyes, methyl orange (MO) is used in a wide range of sectors such as food, textiles, medicine, and printing because it is a dye that is easily soluble in water [4,5].

It is well known that azo dyes cause cancer due to the carcinogenic organic substances they contain [6,7]. Therefore, the removal of MO from wastewater is an extremely significant research topic. The scientific community has recognized the severity of this human-induced problem and is actively engaged in ongoing research efforts to address it. Presently, several established water treatment technologies are in use, including adsorption, membrane separation, chlorination, filtration, electrodialysis, and advanced oxidation processes (AOP) [8]. Notably, AOPs such as Fenton, sonochemical, and photocatalysis have proven highly effective in degrading wastewater pollutants [9–13]. In this context, photocatalysis, a natural phenomenon wherein a material utilizes light energy to cleanse its surface by removing pollutants and harmful compounds, has garnered significant attention. Photocatalysis is considered to be the most efficient strategy among AOPs as it can effectively mineralize existing wastes in the gas or liquid phase [14]. The concept of photocatalysis was

[1]Department of Chemistry, College of Sciences Koç University, 34450 Istanbul Türkiye, [2]Koç University Surface Science and Technology Center (KUYTAM) 34450 Istanbul Türkiye
[#]Corresponding author: zeroglu@ku.edu.tr (Z. Eroglu); ometin@ku.edu.tr (O. Metin)

Keywords: Graphitic Carbon Nitride; 2D Bismuth; Heterojunction; Photodegradation; Sustainable Chemistry.

Received: 09 November 2023 | Accepted: 03 December 2023 | Published: 22 December 2023

introduced by Fujishima and Honda in 1972 when they demonstrated the generation of hydrogen through a photoassisted electrochemical water-splitting reaction, a milestone in the field [15]. Since that seminal work, photocatalysis has undergone extensive research and development. In this process, a photocatalyst, typically a semiconducting material or a hybrid/composite of a semiconductor and conducting material, is excited by light from an external light source, initiating a series of photoinduced reactions [15,16]. Among the various semiconductors commonly investigated in the literature materials such as titanium dioxide (TiO_2) [17], zinc oxide (ZnO) [18], manganese dioxide (MnO_2) [19], tungsten disulfide (WS_2) [20], Black Phosphorus (BP) [21], and graphitic carbon nitride (gCN) [22–24] have gained significant prominence. Notably, gCN, a polymeric semiconductor material composed mainly of carbon (C), nitrogen (N), and hydrogen (H) atoms, characterized by a band gap of 2.7 eV (corresponding to a wavelength of 454 nm), has attracted as a subject of considerable interest in a wide range of photocatalytic applications [25]. The exceptional attributes of gCN, including its low cost-effectiveness, non-toxic nature, apparent stability, and efficient semiconductor properties under both visible and ultraviolet light, have led to its widespread utilization across a spectrum of catalytic applications. These encompass critical processes such as oxygen reduction reaction, water splitting, photodegradation of organic pollutants, and CO_2 reduction [26–30]. While gCN serves as a versatile photocatalyst, it is afflicted by issues of elevated charge recombination rates and insufficient electrical conductivity. Augmenting the photocatalytic performance of semiconductor materials can be effectively achieved through the formation of heterojunctions, a process that facilitates the separation of electron-hole pairs. Consequently, numerous gCN-based heterojunctions have been documented, encompassing associations with various materials such as metals, metal alloys, metal oxides, and other metal-free semiconductor materials [31–33]. Besides gCN, in recent years, there has been a growing interest in two-dimensional (2D) monoelementel materials synthesized with group 15 elements, namely 2D pnictogens (phosphorene, arsenene, antimonene, and bismuthene), due to their attractive properties such as wide and tunable band gaps, high charge mobility, unique spin-orbit coupling (SOC), and their use in many fields such as photonics, optoelectronics, catalysis (electro- and photocatalysis) and biotechnology [34,35]. One of the primary factors driving the significant interest in 2D phosphorene materials lies in their distinctive structural arrangement, resulting in anisotropic properties exhibited by the individual layers. Among 2D materials, 2D Bismuth(2D Bi), which comprises mono/few layers and is distinguished by its robust stability, exceptional electron mobility, and low toxicity, presents intriguing prospects for employment in photocatalytic applications [36]. These prospects stem from its 2D hexagonal lattice structure, narrow band gap, and substantial surface area. Notably, 2D Bi possesses semi-conductive properties, characterized by a tunable bandgap ranging from 0.3 to 1.0 eV when the exfoliated layers are less than 30 nm in thickness [37]. As previously discussed in the context of gCN, the establishment of heterojunctions offers a potential solution to circumvent the limitations associated with 2D Bi as a photocatalyst. Consequently, the investigation of 2D Bi/gCN heterojunctions presents a promising avenue for the development of sustainable photocatalysts with tailored characteristics. To the best of the authors' knowledge, no fields have documented instances of the application of 2D Bi/gCN heterojunctions as photocatalysts. In the present study, a highly effective photocatalyst was prepared by combining 2D Bi and gCN in a binary heterojunction structure with different ratios (denoted as 2D Bi_x/gCN hereafter) via the *in situ* synthesis protocol. The resulting 2D Bi_x/gCN heterojunctions were subjected to comprehensive characterization employing advanced analytical techniques. Subsequently, their photocatalytic performance was assessed in the Methyl Orange (MO) degradation under visible light irradiation. The 2D Bi_x/gCN heterojunctions were exhibited to be an efficient photocatalyst that can be operated under visible light irradiation for photocatalytic dye degradation from water with high product yields compared to gCN. Furthermore, the study included the development of a band diagram elucidating the electron-hole migration dynamics within the gCN and 2D Bi heterojunctions.

2. Results and Discussion

To prepare the 2D Bi_x/gCN heterojunctions (Figure 7), a facile *in situ* synthesis protocol was utilized for the first time. In the synthesis protocol, urea and $BiCl_3$ were mixed in ethanol solution and the resultant mixed powder was pyrolyzed under Argon gas flow. During the synthesis, urea was converted to the polymeric graphitic carbon nitride along with the reduction of Bi(II) ions to the metallic bismuth or 2D Bi. To unveil the structural, morphological, and photophysical properties of gCN, 2D Bi, and the 2D Bi_x/gCN heterojunctions, we conducted a comprehensive set of characterizations, including powder X-ray diffraction (p-XRD), transmission electron microscopy (TEM), high-angle annular dark-field

NANOSAM
Journal of NanoScience in Advanced Materials

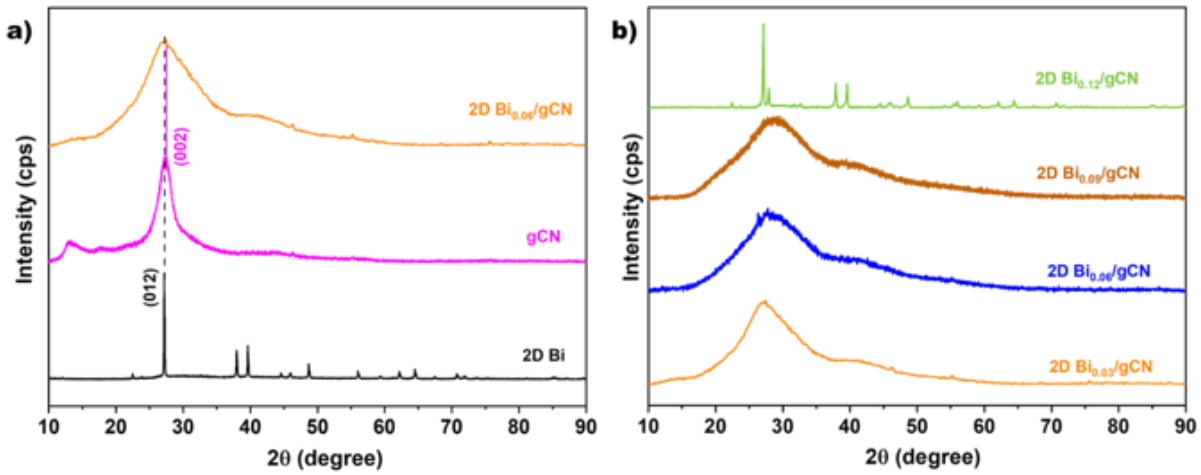

Figure 1. XRD patterns of a) Biene, gCN, and 2D $Bi_{0.06}$/gCN heterojunction, b) different compositions of 2D Bi_x/gCN heterojunctions.

scanning TEM (HAADF-STEM), diffuse reflection spectroscopy (DRS), Tauc plot analysis, photoluminescence (PL), and time-resolved photoluminescence (TRPL).

The crystal structure of 2D Bi_x/gCN heterojunctions was investigated through XRD analysis. The XRD pattern of pristine gCN shows two diffraction peaks at 2θ = 13.0° and 27.4°, corresponding to the (100) and (002) planes, respectively [40]. Furthermore, the XRD pattern of 2D Bi suggests a rhombohedral crystal structure, with diffraction peaks detected at 2θ = 39.6°, 27.2°, and 37.9° assigned to the (110), (012), and (104) planes, respectively (PDF Card no: 04-006-7762) [41]. Figure 1a distinctly illustrates the prominent peaks corresponding to the (012) plane of Biene and the (002) plane of gCN. The XRD pattern also indicates that the synthesized 2D $Bi_{0.06}$/gCN heterojunctions exhibit the characteristic features of both gCN and Biene, with a discernible broad peak observed at 2θ = 27.81°. In the XRD pattern of 2D $Bi_{0.06}$/gCN (Figure 1a), no discernible peaks corresponding to 2D Bi are observed, likely due to the low loading ratio of 2D Bi in the nanocomposite. Upon close examination of XRD patterns for various compositions of 2D Bi_x/gCN heterojunctions in Figure 1b, it becomes evident that the 2D $Bi_{0.03}$/gCN and 2D $Bi_{0.09}$/gCN heterojunctions exhibit predominant peaks characteristic of gCN, while the 2D $Bi_{0.12}$/gCN composition displays the distinctive peaks associated with 2D Bi. As a result of the XRD analysis of 2D Bi/gCN heterojunctions, the incorporation of both gCN and 2D Bi components in the synthesized materials along with variations in the loading ratio of 2D Bi affecting the characteristic peaks observed in the XRD patterns were concluded.

The morphological characteristics of the materials used in the study were examined by TEM

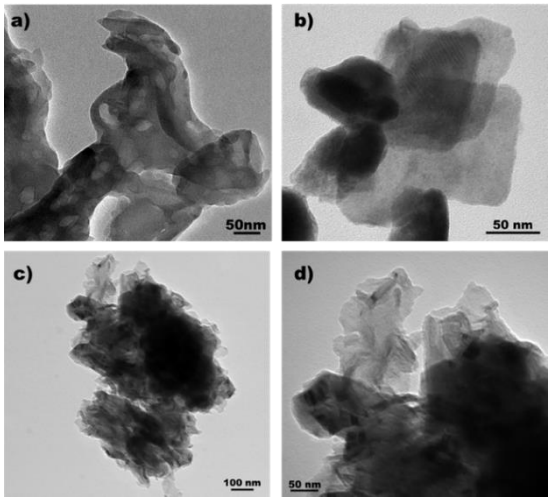

Figure 2. TEM images of a) gCN, b) 2D Bi, and c-d) 2D $Bi_{0.06}$/gCN heterojunction.

analysis. In Figure 2a, the TEM image of gCN demonstrates its mesoporous structure [42], while Figure 2b presents a TEM image of ultrathin 2D Bi with a size of approximately 100 nm [43]. The morphologies of both 2D Bi nanosheets and gCN are depicted in Figure 2c-d. Upon the formation of the 2D $Bi_{0.06}$/gCN heterojunction, no discernible changes in the morphologies of the 2D Bi nanosheets and gCN were observed. Notably, the images reveal the presence of 2D Bi formed between the layers of gCN. These observations validate the successful formation of the desired heterojunction morphological structure through the new synthesis method. Elemental mapping analysis was performed to further investigate the elemental composition of the 2D $Bi_{0.06}$/gCN heterojunction via HAADF-STEM. By examining the HAADF-STEM analysis images in Figure 3, it is clearly observed that the Bi, C, and N elements in the structure are evenly distributed within the 2D $Bi_{0.06}$/gCN heterojunctions.

NANOSAM
Journal of NanoScience in Advanced Materials

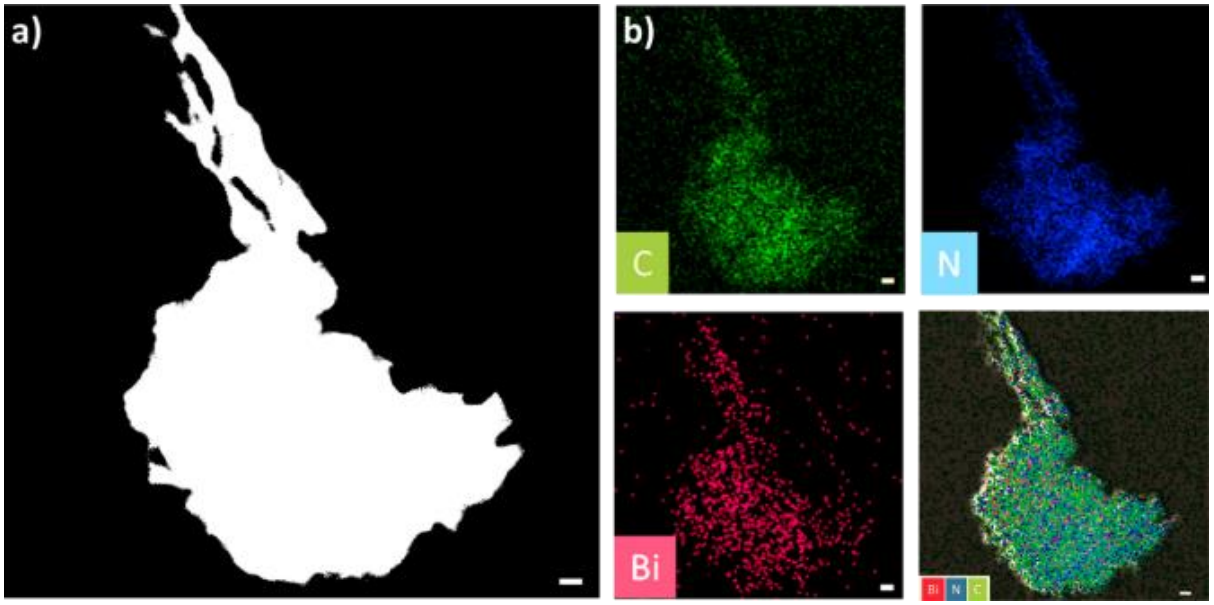

Figure 3. a) HAADF-STEM image, and b) corresponding EDS elemental mapping images of 2D $Bi_{0.06}$/gCN heterojunction (The scale bars are 100 nm).

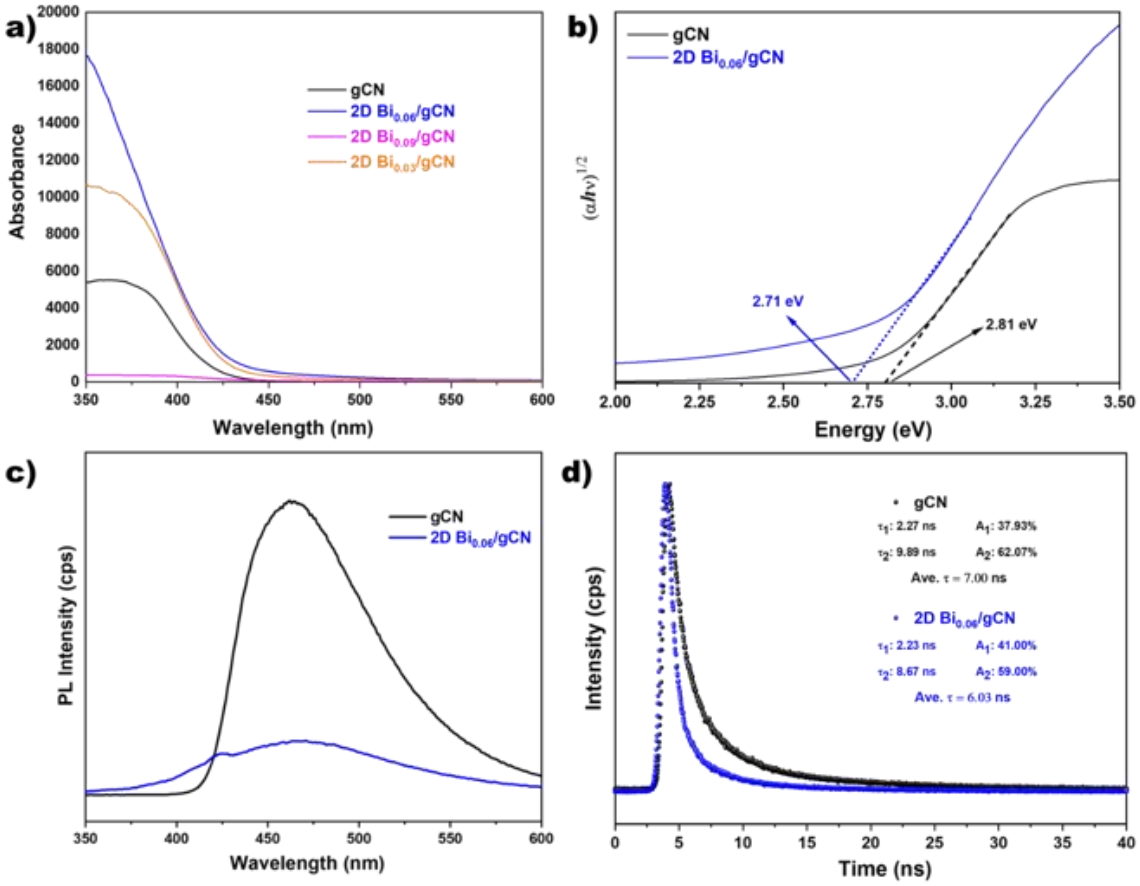

Figure 4. a) Diffuse reflection spectroscopy (DRS) spectra of gCN and 2D Bi_x/gCN heterojunctions, b) Tauc plot, c) steady state PL spectra, and d) time-resolved photoluminescence (TRPL) spectra of gCN and 2D $Bi_{0.06}$/gCN heterojunction.

To assess the photophysical properties of the synthesized 2D Bi_x/gCN heterojunctions, DRS, tauc plot, PL, and TRPL analysis were examined as depicted in Figure 4. DRS analysis, presented in Figure 5a, was conducted to analyze the UV-vis light absorption capability. The results revealed that the

NANOSAM
Journal of NanoScience in Advanced Materials

2D $Bi_{0.06}$/gCN heterojunction exhibited significantly enhanced light absorption at 350 nm, surpassing not only pristine gCN but also other synthesized 2D Bi_x/gCN heterojunctions. Using the Kubelka-Munk theory for indirect semiconductors, the band gap of the 2D $Bi_{0.06}$/gCN heterojunction, which demonstrated the highest absorbance, was determined to be 2.71 eV (Figure 4b). In the steady-state PL spectrum presented in Figure 4c, it is observed that the PL intensity of 2D $Bi_{0.06}$/gCN is considerably lower than that of gCN, indicating more efficient charge separation in 2D $Bi_{0.06}$/gCN compared to gCN [44]. TRPL was employed to evaluate charge kinetics and mobility of the materials with results presented in Figure 4d. The average lifetime of the 2D $Bi_{0.06}$/gCN heterojunction decreased from 7.00 ns to 6.03 ns when compared to gCN. This decrease in both PL, and TRES suggests reduced recombination in 2D $Bi_{0.06}$/gCN, confirming enhanced photocatalytic efficiency [45].

Photodegradation experiments were conducted using MO to investigate the photocatalytic activity of the obtained heterojunction. The photocatalytic performance was assessed by degrading 5mg/L of MO solution using 20 mg of photocatalyst at 25 °C in a homemade photoreactor under visible light irradiation. Initially, the photocatalysts were introduced into the aqueous solution containing the organic pollutant. Following optimization of the adsorption-desorption equilibrium duration, visible light irradiation was initiated, and UV-vis absorbance values were recorded at regular intervals. The comparison of photocatalytic activities was established over a 30-minute period for the degradation of methyl orange (MO) under visible light exposure. Subsequently, utilizing a calibration curve for the time-dependent MO concentration, the photodegradation efficiency was quantified. Among the photocatalytic materials investigated, 2D Bi exhibited a minimal degradation efficiency, consistent with its known sensitivity to water. In contrast, gCN exhibited an initial degradation of MO for up to 5 minutes, resulting in a 36% reduction in 30 minutes. The introduction of 2D $Bi_{0.03}$ into gCN resulted in a modest improvement, achieving a 41% degradation efficiency (Figure 5a). The 2D $Bi_{0.09}$/gCN composite similarly enhanced the degradation yield to 56% compared to pristine gCN, attributed to improved photophysical properties. Notably, the 2D $Bi_{0.06}$/gCN heterojunction demonstrated the highest photocatalytic performance among all tested materials, achieving a 61% MO photodegradation efficiency. As evidenced by the distinctive features in the DRS spectrum, illustrated in Figure 4a, it is noteworthy that 2D $Bi_{0.06}$/gCN exhibits the utmost relative absorbance capacity among the synthesized heterojunction structures. Consequently, owing to this heightened absorbance capacity, 2D $Bi_{0.06}$/gCN demonstrates superior efficiency in contrast to heterojunction configurations characterized by a higher concentration of 2D Bi. This observation underscores the pivotal role of optimal 2D Bi loading in enhancing the absorption capabilities of the heterojunction, consequently influencing its overall photocatalytic performance. Furthermore, our previous study showed that the percentage of self-degradation of MO, i.e. photolysis, was 0.6% [46]. To analyze the kinetics of the photocatalytic reaction, pseudo-first-order kinetics ($\ln(C_0/C_t) = kt$) were applied. According to this kinetic equation, the rate constant (k) for 2D $Bi_{0.06}$/gCN was determined as 0.0162 min^{-1}, representing a 2.04-fold increase in degradation rate compared to gCN for MO photodegradation.

The plausible mechanisms using photocatalysts underlying the degradation of dye are delineated herein (Equations 1-6) [47,48]. Following the generation of photoinduced electron-hole (e^-/h^+) pairs, O_2 molecules in the reaction medium adsorbed onto the surface of photocatalysts. Then the conduction band (CB) tends to appropriate the photoinduced electrons, giving rise to superoxide radicals ($\bullet O_2-$) (Equations 1 and 2). These radicals, in turn, play a pivotal role in the decomposition of dye molecules. Nevertheless, unstable superoxide radicals, which cannot readily engage with dye molecules in an aqueous environment, undergo a transformation into hydroxyl radicals (•OH) through specific reactions (Equations 3 and 4). The resultant hydroxyl radicals adsorb onto the catalyst surface, contributing to the disruption of dye molecules. Conversely, the holes (h+) residing in the valence band (VB) of photocatalysts can either directly dismantle MO molecules or engage in reactions with H_2O to generate hydroxyl radicals. This dualistic interplay of superoxide radicals and holes underscores the intricate pathways through which dye degradation is facilitated in the presence of photocatalysts.

$$2D\ Bi/gCN + h\upsilon \rightarrow e^- + h^+ \quad (1)$$
$$e^- + O_2 \rightarrow \cdot O_2^- \quad (2)$$
$$\cdot O_2^- + 2H^+ + e^- \rightarrow H_2O_2 \quad (3)$$
$$H_2O_2 + e^- \rightarrow \cdot OH + OH^- \quad (4)$$
$$h^+ + H_2O \rightarrow \cdot OH + H^+ \quad (5)$$
$$h^+/\cdot OH/\cdot O_2^- + pollutans \rightarrow intermediate \rightarrow CO_2 + H_2O \quad (6)$$

In the context of the proposed mechanism of MO photodegradation using the 2D Bi_x/gCN photocatalyst, a visual representation is provided in Figure 6. Band potentials for both gCN and 2D Bi were established based on comprehensive research

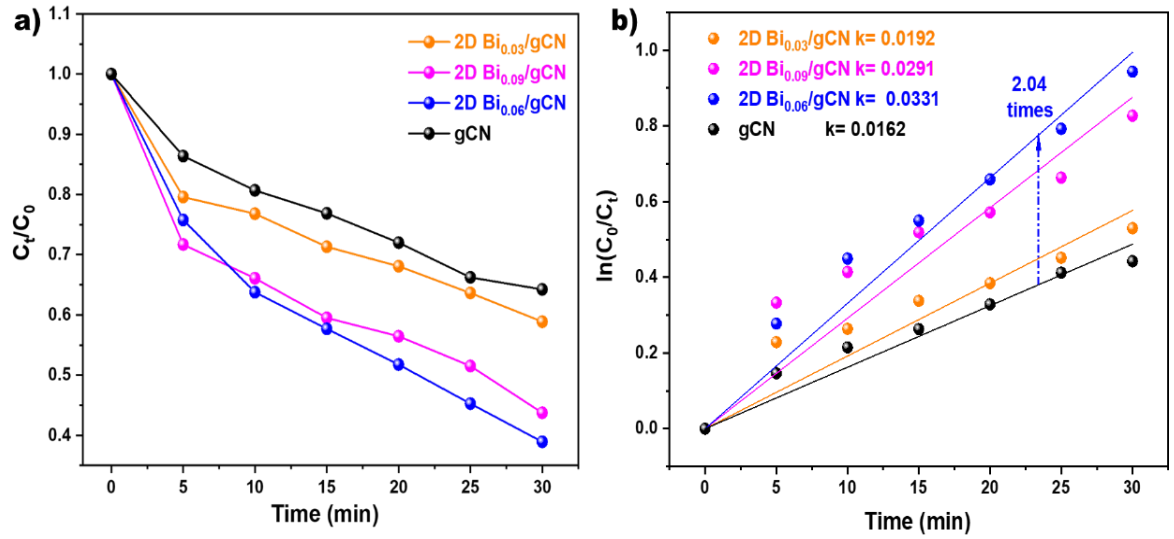

Figure 5. a) Photodegradation of MO under visible-light irradiation with gCN, and 2D Bi_x/gCN b)Pseudo first-order kinetic fitting curves and the corresponding apparent rate constants (K_{app}).

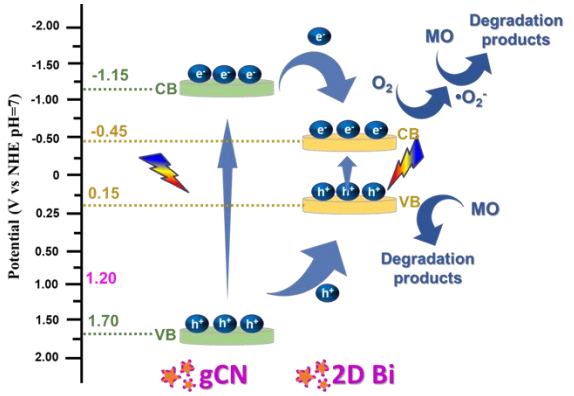

Figure 6. Plausible reaction mechanism of 2D Bi_x/gCN.

conducted by our group [37,49]. Upon exposure to visible light, photogenerated electrons are postulated to migrate from the conduction CB of gCN to 2D Bi. These photoelectrons, present in the CB of 2D Bi, are expected to generate •O_2– necessary for the degradation of organic pollutants [39,50]. Simultaneously, photogenerated holes migrate from the VB of gCN to 2D Bi, which possesses oxidation potentials. This facilitates the conversion of MO into intermediates through an oxidation process with •OH radicals. In light of these findings, we propose that the 2D Bi_x/gCN binary heterojunction functions as a type-I heterojunction, as illustrated by this mechanism.

3. Conclusion

In this study, 2D Bi_x/gCN heterojunctions were successfully synthesized using an *in situ* method. A comprehensive array of characterizations, including p-XRD, TEM, HAADF-STEM, DRS, Tauc plot analysis, PL, and TRPL were performed to investigate the structural, morphological, and photophysical properties of gCN, 2D Bi, and the 2D Bi_x/gCN heterojunction. TEM analysis illustrated the morphological structures of gCN, 2D Bi, and the 2D Bi_x/gCN heterojunctions, confirming the formation of 2D Bi within the gCN layers. Elemental mapping via HAADF-STEM further demonstrated the even distribution of Bi, C, and N elements within the 2D $Bi_{0.06}$/gCN heterojunction. DRS analysis revealed enhanced UV-visible light absorption in the 2D $Bi_{0.06}$/gCN heterojunction, leading to a reduced band gap of 2.71 eV, indicative of efficient light harvesting. PL results indicated improved charge separation in 2D $Bi_{0.06}$/gCN compared to gCN. Photodegradation experiments using MO as a model pollutant showed that 2D Bi had minimal degradation efficiency, while gCN displayed an initial degradation rate, resulting in a 36% reduction of MO in 30 minutes. The introduction of 2D $Bi_{0.03}$/gCN slightly improved the degradation efficiency to 41%. The 2D $Bi_{0.09}$/gCN composite achieved a 56% degradation yield, attributed to enhanced photophysical properties. Notably, the 2D $Bi_{0.06}$/gCN heterojunction exhibited the highest photocatalytic performance, with a 61% MO photodegradation efficiency. Kinetic analysis using pseudo-first-order kinetics revealed a rate constant of 0.0162 min^{-1} for 2D $Bi_{0.06}$/gCN, which was 2.04 times faster than gCN for MO photodegradation. In summary, the synthesized 2D Bi_x/gCN heterojunctions exhibited promising structural, morphological, and photophysical properties, with the 2D $Bi_{0.06}$/gCN heterojunction standing out as a highly efficient photocatalyst for MO degradation under visible light irradiation.

Method

Materials

Bismuth (III) chloride ($BiCl_3$, 98+%), and methyl orange (MO, 96%) were obtained from Sigma-Aldrich. Urea (CH_4N_2O) (99%) was supplied by Merck. Ethyl alcohol (EtOH, absolute, 99.9%) was received from iso-Lab chemicals. All chemicals and solvents were used as received without further purification unless it is noted.

Synthesis of 2D Bi_x/gCN

2D Bi_x/gCN heterojunctions were produced via the in-situ synthesis method by combining graphitic carbon nitride (gCN) and 2D Bi at different ratios. In a typical synthesis of 2D Bi_x/gCN heterojunctions, urea, and $BiCl_3$ were dissolved in 20 ml ethanol in a 100 ml round bottom flask under vigorous stirring with a magnetic stirring bar. The resultant mixture was kept overnight in an oil bath at 80 °C. The obtained powders were placed into a horizontal quartz furnace and treated with the set program as follows: 250 °C in 50 min with a heating rate of 5 °C/min in an N_2 gas atmosphere and kept at this temperature for 2 h. After naturally cooling down to room temperature, the 2D Bi_x/gCN heterojunctions were obtained as a powder. For the preparation of other 2D Bi_x/gCN compositions, 0.03, 0.06, 0.09, and 0.12 mmol of $BiCl_3$ were used in the presence of the constant amount of urea (2 g). The obtained products were labeled as 2D Bi_x/gCN (x is the mmol of $BiCl_3$ precursor used, x = 0.03, 0.06,0.09, and 0.12). To synthesize pristine gCN and 2D Bi for comparison with the binary heterojunction, we employed modified strategies that were previously developed by our research group [38,3].

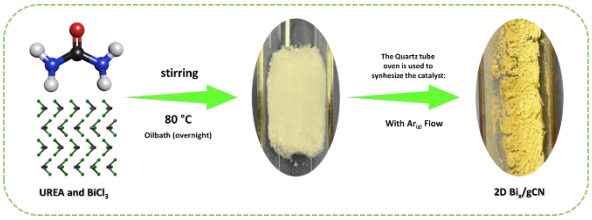

Figure 7. A schematic representation of the preparation of 2D Bi_x/gCN.

Photocatalytic dye degradation experiments

The photocatalytic performance of 2D Bi_x/gCN heterojunctions was tested in the methyl orange (MO, 5 mg/L) degradation in a 100 mL quartz photoreactor under visible light irradiation. A metal halide lamp (150 W with a UV block) was placed in a homemade photocatalytic system. Next, 20 mg of photocatalyst was added to vials and sonicated for 15 min. Following this, the yielded dispersed photocatalysts were added into 100 mL 5 ppm MO solution and stirred in the dark for 30 min to reach adsorption-desorption equilibrium at room temperature and normal pH. Approximately 3 ml of sample was filtered every 5 minutes using a 0.20 µm syringe filter and the absorbance was measured at regular intervals. After determining the optimum time for adsorption and desorption equilibrium, which was 30 minutes, the experiment was continued by turning on the light source and measuring the UV-vis absorbance values for 30 minutes. The degradation efficiency was then calculated from these measurements.

Materials characterization

A Hitachi HT7700 with EXALENS (120 kV) working in high resolution (HR) mode was used to obtain TEM images, HAADF scanning transmission microscope images, and associated EDS elemental mapping images. The Bruker D8 Advance X-ray diffractometer using Cu Kα radiation (1.54 Å) was used to study the X-ray diffraction (XRD) patterns. Photoluminescence (PL) spectroscopy was measured using the Agilent Cary Eclipse PL (320 nm). The nanomaterials were subjected to time-resolved photoluminescence (TRPL) spectroscopy using an Edinburgh Instruments FLS1000 spectrometer (377 nm). Diffuse reflectance ultraviolet-visible-near-infrared (UV-Vis-NIR) spectroscopy was used to study the absorption characteristics using a Shimadzu UV-3600 UV-Vis-NIR spectrophotometer.

Acknowledgements

Ö.M. thanks to The Turkish Academy of Sciences (TÜBA) for the financial support.

Authors' contributions:

B.S.: Conceptualization, formal analysis, methodology, validation, investigation, writing - original draft, visualization.

A. T.: Formal analysis, methodology, investigation,

Z.E.: Conceptualization, formal analysis, methodology, validation, investigation, writing-review&editing, supervision, visualization,

O.M.: Conceptualization, writing- review&editing, supervision, funding acquisition, project administration, provision.

Declaration of Competing Interests

The authors declare that they have no known competing financial interests or personal

NANOSAM
Journal of NanoScience in Advanced Materials

relationships that could have appeared to influence the work reported in this paper.

Data Availability Statement

The data that support the findings of this study are available from the corresponding author upon reasonable request.

References

[1] Ukaogo, P. O.; Ewuzie, U.; Onwuka, C. V. Environmental Pollution: Causes, Effects, and the Remedies. In Microorganisms for Sustainable Environment and Health; Elsevier, 419–429 (2020).

[2] Shang, Y.; Xu, A. An Evaluation of the Impact of Natural Ecotourism on Environmental Pollution. Environ. Sci. Pollut. Res **28** (26), 33764–33770 (2021).

[3] Lu, G.; Li, X.; Li, W.; Liu, Y.; Wang, N.; Pan, Z.; Zhang, G.; Zhang, Y.; Lai, B. Thermo-Activated Periodate Oxidation Process for Tetracycline Degradation: Kinetics and Byproducts Transformation Pathways. J. Hazard. Mater. **461**, 132696 (2024).

[4] Dey, P. C.; Das, R. Enhanced Photocatalytic Degradation of Methyl Orange Dye on Interaction with Synthesized Ligand Free CdS Nanocrystals under Visible Light Illumination. Spectrochim. Acta Part A Mol. Biomol. Spectrosc. **231**, 118122 (2020).

[5] Mittal, A.; Malviya, A.; Kaur, D.; Mittal, J.; Kurup, L. Studies on the Adsorption Kinetics and Isotherms for the Removal and Recovery of Methyl Orange from Wastewaters Using Waste Materials. J. Hazard. Mater. **148** (1–2), 229–240 (2007).

[6] Combes, R. D.; Haveland-Smith, R. B. A Review of the Genotoxicity of Food, Drug and Cosmetic Colours and Other Azo, Triphenylmethane and Xanthene Dyes. Mutat. Res. Genet. Toxicol. **98** (2), 101–243 (1982).

[7] Prival, M. J.; Davis, V. M.; Peiperl, M. D.; Bell, S. J. Evaluation of Azo Food Dyes for Mutagenicity and Inhibition of Mutagenicity by Methods Using Salmonella Typhimurium. Mutat. Res. Toxicol. **206** (2), 247–259 (1988).

[8] Zou, Y.; Wang, X.; Khan, A.; Wang, P.; Liu, Y.; Alsaedi, A.; Hayat, T.; Wang, X. Environmental Remediation and Application of Nanoscale Zero-Valent Iron and Its Composites for the Removal of Heavy Metal Ions: A Review. Environ. Sci. Technol. **50** (14), 7290–7304 (2016).

[9] Yang, S.; Tian, D.; Wang, X.; Zhou, P.; Xiong, Z.; Zhang, H.; Liu, Y.; Yao, G.; Lai, B. The Enhanced Mechanism of Fe(III)/H2O2 System by N, S-Doped Mesoporous Nanocarbon for the Degradation of Sulfamethoxazole. Sep. Purif. Technol. **308**, 122900 (2023).

[10] Yin, K.; Wu, R.; Shang, Y.; Chen, D.; Wu, Z.; Wang, X.; Gao, B.; Xu, X. Microenvironment Modulation of Cobalt Single-Atom Catalysts for Boosting Both Radical Oxidation and Electron-Transfer Process in Fenton-like System. Appl. Catal. B Environ. **329**, 122558 (2023).

[11] Yin, K.; Peng, L.; Chen, D.; Liu, S.; Zhang, Y.; Gao, B.; Fu, K.; Shang, Y.; Xu, X. High-Loading of Well Dispersed Single-Atom Catalysts Derived from Fe-Rich Marine Algae for Boosting Fenton-like Reaction: Role Identification of Iron Center and Catalytic Mechanisms. Appl. Catal. B Environ. **336**, 122951 (2023).

[12] Shang, Y.; Kan, Y.; Xu, X. Stability and Regeneration of Metal Catalytic Sites with Different Sizes in Fenton-like System. Chinese Chem. Lett. **34** (8), 108278 (2023).

[13] Yang, M.; Hou, Z.; Zhang, X.; Gao, B.; Li, Y.; Shang, Y.; Yue, Q.; Duan, X.; Xu, X. Unveiling the Origins of Selective Oxidation in Single-Atom Catalysis via Co–N 4 –C Intensified Radical and Nonradical Pathways. Environ. Sci. Technol. **56** (16), 11635–11645 (2022).

[14] Ahmad, R.; Ahmad, Z.; Khan, A. U.; Mastoi, N. R.; Aslam, M.; Kim, J. Photocatalytic Systems as an Advanced Environmental Remediation: Recent Developments, Limitations and New Avenues for Applications. Journal of Environmental Chemical Engineering. Elsevier Ltd December 1, 4143–4164 (2016).

[15] Fujishima, A., Honda, K. Electrochemical Photolysis of Water at a Semiconductor Electrode. Nature **238** (5358), 37–38 (1972).

[16] Hunge, Y. M. Basics and Advanced Developments in Photocatalysis – a Review (Mini Review). Int. J. Hydrol. **2** (4) (2018).

[17] Sun, R.; Wang, Z.; Saito, M.; Shibata, N.; Ikuhara, Y. Atomistic Mechanisms of Nonstoichiometry-Induced Twin Boundary Structural Transformation in Titanium Dioxide. Nat. Commun. **6** (1), 7120 (2015).

[18] Yano, M.; Koike, K.; Ogata, K.; Nogami, T.; Tanabe, S.; Sasa, S. Zinc Oxide-based Biosensors. Phys. status solidi c **9** (7), 1570–1573 (2012).

[19] Zhu, M.; Hu, Y.; Li, Y.; Jin, H.; Zhu, Z. Effect of Magnetic Field on Phase Morphology Transformation of MnO 2 Nanostructures in a Hydrothermal Process. Phys. status solidi c **9** (1), 122–127 (2012).

[20] Pandey, K.; Jeong, H. K. Synthesis of Tungsten Disulfide for Electrochemical Energy Applications. Mater. Sci. Eng. B 295, 116601 (2023).

[21] Sakthivel, T.; Huang, X.; Wu, Y.; Rtimi, S. Recent Progress in Black Phosphorus Nanostructures as Environmental Photocatalysts. Chem. Eng. J. **379**, 122297 (2020).

[22] Jiang, L.; Yuan, X.; Pan, Y.; Liang, J.; Zeng, G.; Wu, Z.; Wang, H. Doping of Graphitic Carbon Nitride for Photocatalysis: A Review. Appl. Catal. B Environ. **217**, 388–406 (2017).

[23] Wang, X.; Blechert, S.; Antonietti, M. Polymeric Graphitic Carbon Nitride for Heterogeneous Photocatalysis. ACS Catal. **2** (8), 1596–1606 (2012).

[24] Cao, S.; Low, J.; Yu, J.; Jaroniec, M. Polymeric Photocatalysts Based on Graphitic Carbon Nitride. Adv. Mater. **27** (13), 2150–2176 (2015).

[25] Zhou, L.; Zhang, H.; Sun, H.; Liu, S.; Tade, M. O.; Wang, S.; Jin, W. Recent Advances in Non-Metal Modification of Graphitic Carbon Nitride for Photocatalysis: A Historic Review. Catal. Sci. Technol. **6** (19), 7002–7023 (2016).

[26] Nasir, M. S.; Yang, G.; Ayub, I.; Wang, S.; Wang, L.; Wang, X.; Yan, W.; Peng, S.; Ramakarishna, S. Recent Development in Graphitic Carbon Nitride Based Photocatalysis for Hydrogen Generation. Appl. Catal. B Environ. **257**, 117855 (2019).

[27] Zhou, J.; Chen, W.; Sun, C.; Han, L.; Qin, C.; Chen, M.; Wang, X.; Wang, E.; Su, Z. Oxidative Polyoxometalates Modified Graphitic Carbon Nitride for Visible-Light CO 2 Reduction. ACS Appl. Mater. Interfaces **9** (13), 11689–11695 (2017).

[28] Zhang, N.; Wen, L.; Yan, J.; Liu, Y. Dye-Sensitized Graphitic Carbon Nitride (g-C3N4) for Photocatalysis: A Brief Review. Chem. Pap. **74** (2), 389–406 (2020).

[29] Wudil, Y. S.; Ahmad, U. F.; Gondal, M. A.; Al-Osta, M. A.; Almohammedi, A.; Sa'id, R. S.; Hrahsheh, F.; Haruna, K.; Mohamed, M. J. S. Tuning of Graphitic Carbon Nitride (g-C3N4) for Photocatalysis: A Critical Review. Arab. J. Chem. **16** (3), 104542 (2023).

[30] Li, H.; Liu, Y.; Gao, X.; Fu, C.; Wang, X. Facile Synthesis and Enhanced Visible-Light Photocatalysis of Graphitic Carbon Nitride Composite Semiconductors. ChemSusChem **8** (7), 1189–1196 (2015).

[31] Wang, J.; Xu, M.; Tremblay, P.-L.; Zhang, T. Improved Polyhydroxybutyrate Production by Cupriavidus Necator and the Photocatalyst Graphitic Carbon Nitride from Fructose under Low Light Intensity. Int. J. Biol. Macromol. **203**, 526–534 (2022).

[32] Le, S.; Jiang, T.; Zhao, Q.; Liu, X.; Li, Y.; Fang, B.; Gong, M. Cu-Doped Mesoporous Graphitic Carbon Nitride for Enhanced Visible-Light Driven Photocatalysis. RSC Adv. **6** (45), 38811–38819 (2016).

[33] Lin, H.; Wu, J.; Zhou, F.; Zhao, X.; Lu, P.; Sun, G.; Song, Y.; Li, Y.; Liu, X.; Dai, H. Graphitic Carbon Nitride-Based Photocatalysts in the Applications of Environmental Catalysis. J. Environ. Sci. **124**, 570–590 (2023).

[34] Liu, X.; Zhang, S.; Guo, S.; Cai, B.; Yang, S. A.; Shan, F.; Pumera, M.; Zeng, H. Advances of 2D Bismuth in Energy Sciences. Chem. Soc. Rev. **49** (1), 263–285 (2020).

[35] Zhang, K.; Jin, B.; Park, C.; Cho, Y.; Song, X.; Shi, X.; Zhang, S.; Kim, W.; Zeng, H.; Park, J. H. Black Phosphorene as a Hole Extraction Layer Boosting Solar Water Splitting of Oxygen Evolution Catalysts. Nat. Commun. **10** (1), 2001 (2019).

[36] R., S.; Kainthla, I.; Dongre S., S.; D'Souza, L.; Balakrishna, R. G. Recent Advances in Ecofriendly 2D Monoelemental Bismuthene as an Emerging Material for Energy, Catalysis and Biomedical Applications. J. Mater. Chem. C **11** (21), 6777–6799 (2023).

[37] Ozer, M. S.; Eroglu, Z.; Yalin, A. S.; Kılıç, M.; Rothlisberger, U.; Metin, O. Bismuthene as a Versatile Photocatalyst Operating under Variable Conditions for the Photoredox C H Bond Functionalization. Appl. Catal. B Environ. **304**, 120957 (2022).

[38] Yilmazer, A.; Eroglu, Z.; Gurcan, C.; Gazzi, A.; Ekim, O.; Sundu, B.; Gokce, C.; Ceylan, A.; Giro, L.; Unal, M. A.; Arı, F.; Ekicibil, A.; Ozgenç Çinar, O.; Ozturk, B. I.; Besbinar, O.; Ensoy, M.; Cansaran-Duman, D.; Delogu, L. G.; Metin, O. Synergized Photothermal Therapy and Magnetic Field Induced Hyperthermia via Bismuthene for Lung Cancer Combinatorial Treatment. Mater. Today Bio **23**, 100825 (2023).

[39] Eroglu, Z.; Ozer, M. S.; Metin, O. Black Phosphorus Quantum Dots/Carbon Nitride-Reduced Graphene Oxide Ternary Heterojunction as a Multifunctional Metal-Free Photocatalyst for Photooxidation Reactions. ACS Sustain. Chem. Eng. **11** (19), 7560–7572 (2023).

[40] Cao, S.; Low, J.; Yu, J.; Jaroniec, M. Polymeric Photocatalysts Based on Graphitic Carbon Nitride. Adv. Mater. **27** (13), 2150–2176 (2015).

[41] Zhang, W.; Hu, Y.; Ma, L.; Zhu, G.; Zhao, P.; Xue, X.; Chen, R.; Yang, S.; Ma, J.; Liu, J.; Jin, Z. Liquid-Phase Exfoliated Ultrathin Bi Nanosheets: Uncovering the Origins of Enhanced Electrocatalytic CO2 Reduction on Two-Dimensional Metal Nanostructure. Nano Energy **53**, 808–816 (2018).

[42] Kong, L.; Wang, J.; Ma, F.; Sun, M.; Quan, J. Graphitic Carbon Nitride Nanostructures: Catalysis. Appl. Mater. Today **16**, 388–424 (2019).

[43] Zhu, Y.; Wu, Y.; Li, S.; Yuan, X.; Shen, J.; Luo, S.; Wang, Z.; Gao, R.; Wu, J.; Ge, L. Photocatalytic and Photothermal Bismuthene Nanosheets as Drug Carrier Capable of Generating CO to Improve Drug Sensitivity and Reduce Inflammation for Enhanced Cancer Therapy. Chem. Eng. J. **446**, 137321 (2022).

[44] Liu, C.; Zhang, Y.; Dong, F.; Reshak, A. H.; Ye, L.; Pinna, N.; Zeng, C.; Zhang, T.; Huang, H. Chlorine Intercalation in Graphitic Carbon Nitride for Efficient Photocatalysis. Appl. Catal. B Environ. **203**, 465–474 (2017).

[45] Fang, X.; Gao, R.; Yang, Y.; Yan, D. A Cocrystal Precursor Strategy for Carbon-Rich Graphitic Carbon Nitride toward High-Efficiency Photocatalytic Overall Water Splitting. iScience **16**, 22–30 (2019).

[46] Eroglu, Z.; Sündü, B.; Metin, O. Tailoring the Redox Ability of Carbon Nitride Quantum Dots/Reduced Graphene Oxide-Black Phosphorus (CNQDs@rGOBP) Ternary Heterojunctions for Photodegradation of Organic Pollutants. Mater. Today Sustain. **23**, 100418 (2023).

[47] Kılıç, D.; Sevim, M.; Eroğlu, Z.; Metin, Ö.; Karaca, S. Strontium Oxide Modified Mesoporous Graphitic Carbon Nitride/Titanium Dioxide Nanocomposites (SrO-Mpg-CN/TiO2) as Efficient Heterojunction Photocatalysts for the Degradation of Tetracycline in Water. Adv. Powder Technol. **32** (8), 2743–2757 (2021).

[48] Altan, O.; Eroğlu, Z.; Küçükkeçeci, H.; Metin, Ö. Black Phosphorus-Based Photocatalysts for Energy and Environmental Applications. In Nanostructured Photocatalysts; Elsevier, 421–449 (2021).

[49] Eroglu, Z.; Ozer, M. S.; Kubanaliev, T.; Kilic, H.; Metin, Ö. Synergism between Few-Layer Black Phosphorus and Graphitic Carbon Nitride Enhances the Photoredox C–H Arylation under Visible Light Irradiation. Catal. Sci. Technol. **12** (17), 5379–5389 (2022).

[50] Eroglu, Z.; Metin, O. Internal Interactions within the Complex Type-II Heterojunction of a Graphitic Carbon Nitride/Black Phosphorus Hybrid Decorated with Graphene Quantum Dots: Implications for Photooxidation Performance. ACS Appl. Nano Mater. **6** (9), 7960–7974 (2023).